Journal of Virology®

VIRUS-CELL INTERACTIONS

ADAM15 Participates in Tick-Borne Encephalitis Virus Replication

Qi Yang,[a,b] Rongjuan Pei,[b] Yun Wang,[b] Yuan Zhou,[b] Min Yang,[a] Xinwen Chen,[b,c] Jizheng Chen[b]

[a]Department of Gastroenterology, Guangzhou Women and Children's Medical Center, Guangzhou, China
[b]State Key Laboratory of Virology, Wuhan Institute of Virology, Center for Biosafety Mega-Science, Chinese Academy of Sciences, Wuhan, China
[c]Guangzhou Regenerative Medicine and Health–Guangdong Laboratory, Guangzhou Institutes of Biomedicine and Health, Chinese Academy of Sciences, Guangzhou, China

ABSTRACT Tick-borne encephalitis virus (TBEV), a major tick-borne viral pathogen of humans, is known to cause neurological diseases such as meningitis, encephalitis, and meningoencephalitis. However, the life cycle and pathogenesis of TBEV are not well understood. Here, we show that the knockdown or knockout of ADAM15 (a disintegrin and metalloproteinase 15), a host protein involved in neuroblastoma diseases, leads to TBEV replication and assembly defects. We characterized the disintegrin domain in ADAM15 and found that the ADAM15 subcellular localization was changed following TBEV infection. RNA interference (RNAi) screen analysis confirmed ADAM's nonredundant functions and identified a specific role for ADAM15 in TBEV infection. An RNA-sequencing analysis was also conducted to understand the causal link between TBEV infection and the cellular endomembrane network, namely, the generation of replication organelles promoting viral genome replication and virus production. Our data demonstrated that TBEV infection changes ADAM15 cellular localization, which contributes to membrane reorganization and viral replication.

IMPORTANCE Tick populations are increasing, and their geographic ranges are expanding. Increases in tick-borne disease prevalence and transmission are important public health issues. Tick-borne encephalitis virus (TBEV) often results in meningitis, encephalitis, and meningoencephalitis. TBEV causes clinical disease in more than 20,000 humans in Europe and Asia per year. An increased incidence of TBE has been noted in Europe and Asia, as a consequence of climate and socioeconomic changes. The need to investigate the mechanism(s) of interaction between the virus and the host factors is apparent, as it will help us to understand the roles of host factors in the life cycle of TBEV. The significance of our research is in identifying the ADAM15 for TBEV replication, which will greatly enhance our understanding of TBEV life cycle and highlight a target for pharmaceutical consideration.

KEYWORDS TBEV, ADAM15, replication, TBEV, assembly, replication

Tick-borne encephalitis virus (TBEV) is a zoonotic flavivirus of the family *Flaviviridae* that is endemic throughout the northern Palearctic, spanning an area from central and northern Europe across Siberia to Japan in the far east (1). TBEV is maintained in a cycle that includes tick vectors of the *Ixodes persulcatus* complex and their vertebrate hosts (2). The most important vector in Central Europe is *Ixodes ricinus*, and small rodents are the most important hosts for the immature stages of *I. ricinus* (3, 4). Over the past 30 years, TBEV has been considered an important tick-borne flavivirus (TBFV) in Europe and Asia and has been a growing public health problem, with approximately 13,000 estimated human cases annually (5).

TBEV belongs to the genus *Flavivirus* in the family *Flaviviridae*. The mature TBEV particles are smooth and have a diameter of 50 nm (6). According to phylogenetic

Citation Yang Q, Pei R, Wang Y, Zhou Y, Yang M, Chen X, Chen J. 2021. ADAM15 participates in tick-borne encephalitis virus replication. J Virol 95:e01926-20. https://doi.org/10.1128/JVI.01926-20.

Editor Rebecca Ellis Dutch, University of Kentucky College of Medicine

Address correspondence to Qi Yang, yangqi@wh.iov.cn, or Jizheng Chen, chenjz@wh.iov.cn.

Received 9 October 2020
Accepted 12 November 2020
Accepted manuscript posted online 18 November 2020
Published 28 January 2021

differences, TBEV has been divided into three main subtypes: the European (TBEV-Eu), Siberian (TBEV-Sib), and Far Eastern (TBEV-FE) subtypes. Recently, two new subtypes were proposed: the Baikalian (TBEV-Bkl) and Himalayan (TBEV-Him) (7, 8) subtypes. The clinical courses of infection differ in the degree of neuroinvasiveness and neurovirulence, which may depend on the different viral subtypes (9). In addition, dendritic transport of TBEV RNA by neuronal granules affects the neurological disease (10). TBEV has an ~11-kb positive-strand RNA genome that encodes a polyprotein precursor, capable of co- and posttranslational proteolytic processing that results in the production of three structural proteins (core [C], membrane [M], and envelope [E]) and seven nonstructural (NS) proteins (NS1, NS2A, NS2B, NS3, NS4A, NS4B, and NS5) (1). Although the TBEV life cycle has been well characterized, the specific host and viral factors and the mechanisms involved in aspects of receptor binding, replication, and viral assembly are poorly understood.

The ADAM (a disintegrin and a metalloproteinase) family of transmembrane and secreted metalloproteinases performs important functions in cell adhesion and signaling, primarily through the regulated ectodomain shedding of ligands and receptors for multiple pathways, such as those controlled by the epidermal growth factor receptor and Notch (11, 12). ADAM15, a multidomain metalloproteinase, has been implicated in the pathogenesis of many human diseases, such as cancer (breast cancer, lung cancer, and neuroblastoma) and inflammatory diseases (11, 13). ADAM15 shares the multidomain organization with other family members containing metalloproteinase (MP), disintegrin, cysteine-rich, and epidermal growth factor (EGF)-like domains, which are connected via a transmembrane helix to the intracellular domain (ICD) (14). ADAM15 is the only member of the ADAM family with the integrin-binding motif Arg-Gly-Asp (RGD) in its disintegrin-like domain, which has important functions in integrin binding (13). ADAM15 is mainly expressed in neuroglia and endothelial cells in human brains. Astrocytes play an important role in neurotropic flaviviruses infection (15). TBEV infection can induce proinflammatory cytokines and chemokines and lead to injury of human astrocytes (16). A recent study has suggested that TBEV affects the development of neurological disease by neuronal granules (10). Hence, in this study we investigated the role of ADAM15 in TBEV infection.

We demonstrate that ADAM15 is a host factor exploited by TBEV. Our data show that ADAM15 plays an important role in neural cells for TBEV replication and the production of infectious virus particles. Additionally, we show that TBEV infection causes ADAM15 localization to change from lipid rafts to the endoplasmic reticulum (ER), and RNA sequencing analysis established a link between ADAM15 and the membrane rearrangements required for replication. In this study, we unveiled unknown possible TBEV host factors and identified ADAM15 as a novel factor supporting TBEV replication.

RESULTS

ADAM15 is involved in the infection of TBEV. It has been widely reported that the ADAM family is involved in viral infection (17–19). We wondered whether ADAMs were involved in the life cycle of TBEV. First, of the 34 ADAM proteins described, including the 20 human ADAMs, RNA sequencing (RNA-Seq) defined ADAM's expression in T98G cells and TBEV-infected T98G cells (Fig. 1A). Only 9 of 20 ADAMs are expressed in these cells, including ADAM8 to -12, -15, -17, -19, and -22. We then confirmed the efficiency of small interfering RNAs (siRNAs) targeting the mRNA transcripts for the nine genes (Fig. 1B) and tested the effects on TBEV infection. In infected cells, only the knockdown of *ADAM15* significantly reduced TBEV RNA levels compared to the control cells expressing nontarget siRNA (Fig. 1C). Additionally, the *ADAM15* knockdown also reduced NS1 protein levels (Fig. 1D). These results suggested that *ADAM15* is necessary for TBEV replication compared with other ADAMs.

Deficiency of *ADAM15* suppresses TBEV replication. We then determined the efficiency of three siRNAs targeting different *ADAM15* mRNA sequences in T98G (Fig. 2A). Knockdown of *ADAM15* resulted in significantly reduced viral RNA, viral titers, and NS1

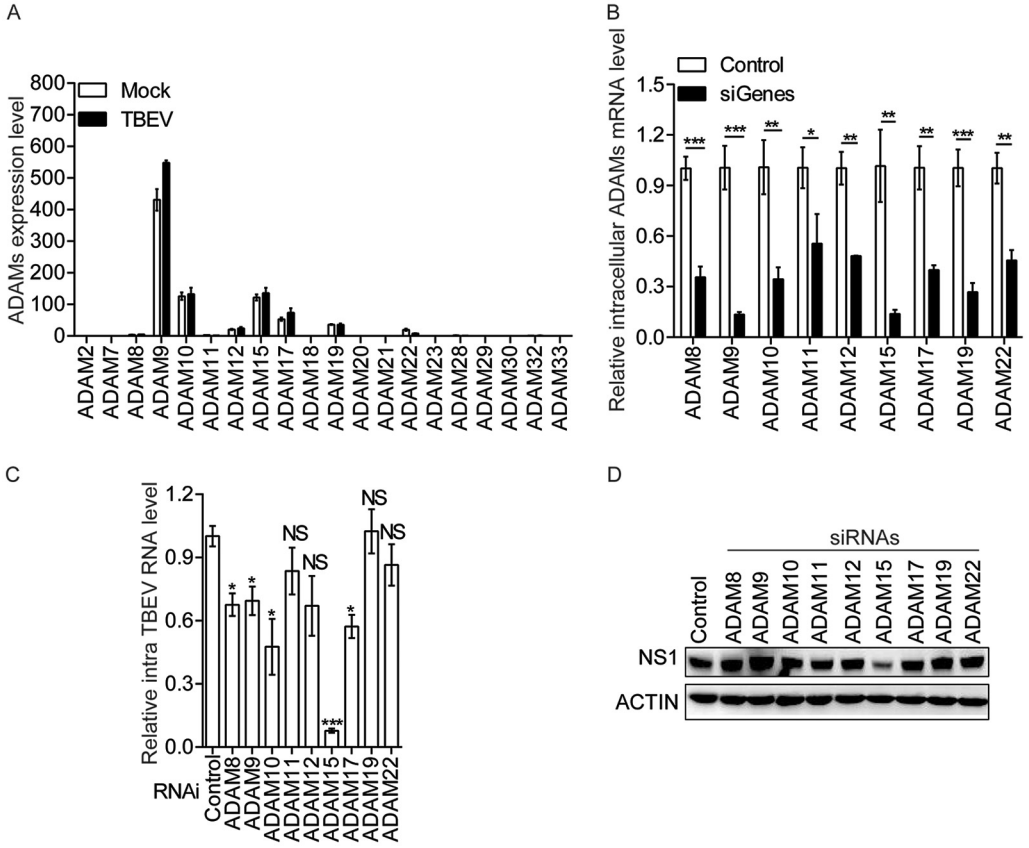

FIG 1 Effects of ADAM protein knockdown on TBEV infection. (A, C, and D) T98G cells were infected with TBEV for 48 h. (A) ADAM expression profiles were evaluated using RNA sequencing. For genomes used, see Data Set S1. (B to D) T98G cells were transfected with siRNAs targeting the indicated mRNA transcripts or with a nontargeting siRNA (control). (B) ADAM8 to -12, -15, -17, -19, and -22 mRNA transcript levels were analyzed by qPCR/RT-PCR, and values were corrected using β-actin. The graph shows average change compared to control for 3 independent experiments. (C) Cells were lysed for TBEV RNA analysis. The graph shows average change relative to control for 3 independent experiments. (D) NS1 protein levels were evaluated by Western blotting. Data are representative of 3 independent experiments; data in the graphs are means and SD. *, $P < 0.05$; **, $P < 0.01$; ***, $P < 0.001$; NS, no significant difference.

levels of TBEV-FE subtype WH2012 following infection of T98G (Fig. 2B to D) without causing cytotoxicity (Fig. 2E). Moreover, *ADAM15* knockdown also reduced the titers of TBEV-Eu subtype Neudoerfl (Fig. 2F). We also found that knockdown of *ADAM15* via siRNAs could inhibit the TBEV replication in U251 cells (data not shown).

Next, we evaluated the effect of *ADAM15* knockout on TBEV infection. We generated *ADAM15*$^{-/-}$ single-cell clones using at least three single guide RNAs (sgRNAs) and validated gene deletion in T98G. In infected cells, knockout of *ADAM15* considerably reduced the TBEV-FE (WH2012) RNA levels, virus titers, and NS1 levels following infection of T98G (Fig. 2G to I) without affecting cell viability (Fig. 2J). *ADAM15* knockout also reduced the TBEV-Eu (Neudoerfl) titers (Fig. 2K). Knockout of *ADAM15* suppressed TBEV replication in U251 cells (data not shown). Altogether, these results suggested that ADAM15 positively regulates the TBEV replication.

Furthermore, we evaluated ADAM15 in multistep growth curves with two TBEV subtypes. Infection of TBEV was reduced in *ADAM15*$^{-/-}$ U251 cells, and transcomplementation of ADAM15 in *ADAM15*$^{-/-}$ U251 cells restored TBEV infectivity (Fig. 3A to D). Finally, we sought to knock down *ADAM15* in mouse primary astrocytes using small interfering RNA (siRNA) duplexes. The *ADAM15* knockdown astrocytes exhibited markedly lower TBEV infection than control primary astrocytes (Fig. 3E). These data indicated that ADAM15 plays a role in virus infection for different cells and TBEV subtypes.

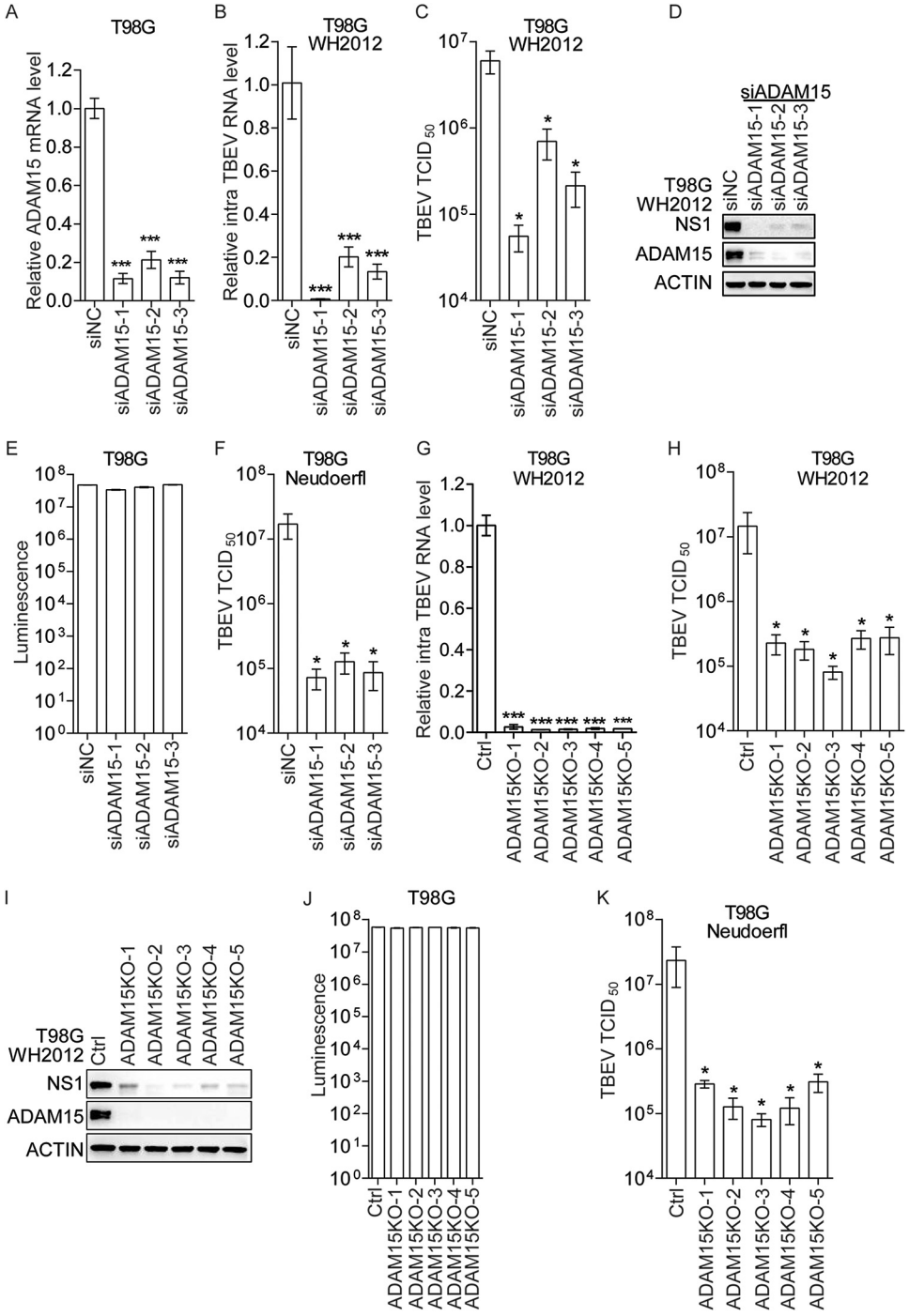

FIG 2 Deficiency of ADAM15 reduces TBEV infection. (A to F) T98G cells were transfected with siRNAs targeting ADAM15 mRNA transcripts or a nontargeting siRNA (control). (A) At 48 h posttransfection, ADAM15 mRNA levels were evaluated in T98G cells. (A) Average change compared to control cells. (B to D) T98G cells were transfected with siNC or siADAM15 for 48 h and then infected with TBEV WH2012 for 48 h. The intracellular viral RNA (B), virus titer (C), and ADAM15/NS1 protein levels (D) were quantified. (B) Mean change in viral RNA levels relative to control cells. (C) Mean change in 50% tissue culture infective doses ($TCID_{50}$) ml^{-1} relative to control cells. (D) WB showed changes in ADAM15 and NS1 protein levels relative to control cells. (E) Cell viability was evaluated in T98G cells. (F) T98G cells were infected with TBEV Neudoerfl for 48 h, and then virus titer was quantified. Data are mean change in $TCID_{50}$ ml^{-1} relative to control cells. (G to I) TBEV WH2012 was used to infect control or ADAM15$^{-/-}$ T98G cells for 48 h. The intracellular viral RNA (G), virus titer (H), and ADAM15/NS1 protein levels (I) were quantified. (G) Mean change in viral RNA levels relative to control cells. (H) Mean change in $TCID_{50}$ ml^{-1} relative to control cells. (I) WB showing changes in ADAM15 and NS1 protein levels relative to control cells. (J) Cell viability was evaluated in T98G cells or ADAM15$^{-/-}$ T98G cells. (K) T98G cells were infected with TBEV Neudoerfl for 48 h, and then virus titer was quantified. Data are mean change in $TCID_{50}$ ml^{-1} relative to control cells. All graphs are representative of 3 independent experiments. Quantitative data are means and SD. *, $P < 0.05$; ***, $P < 0.001$.

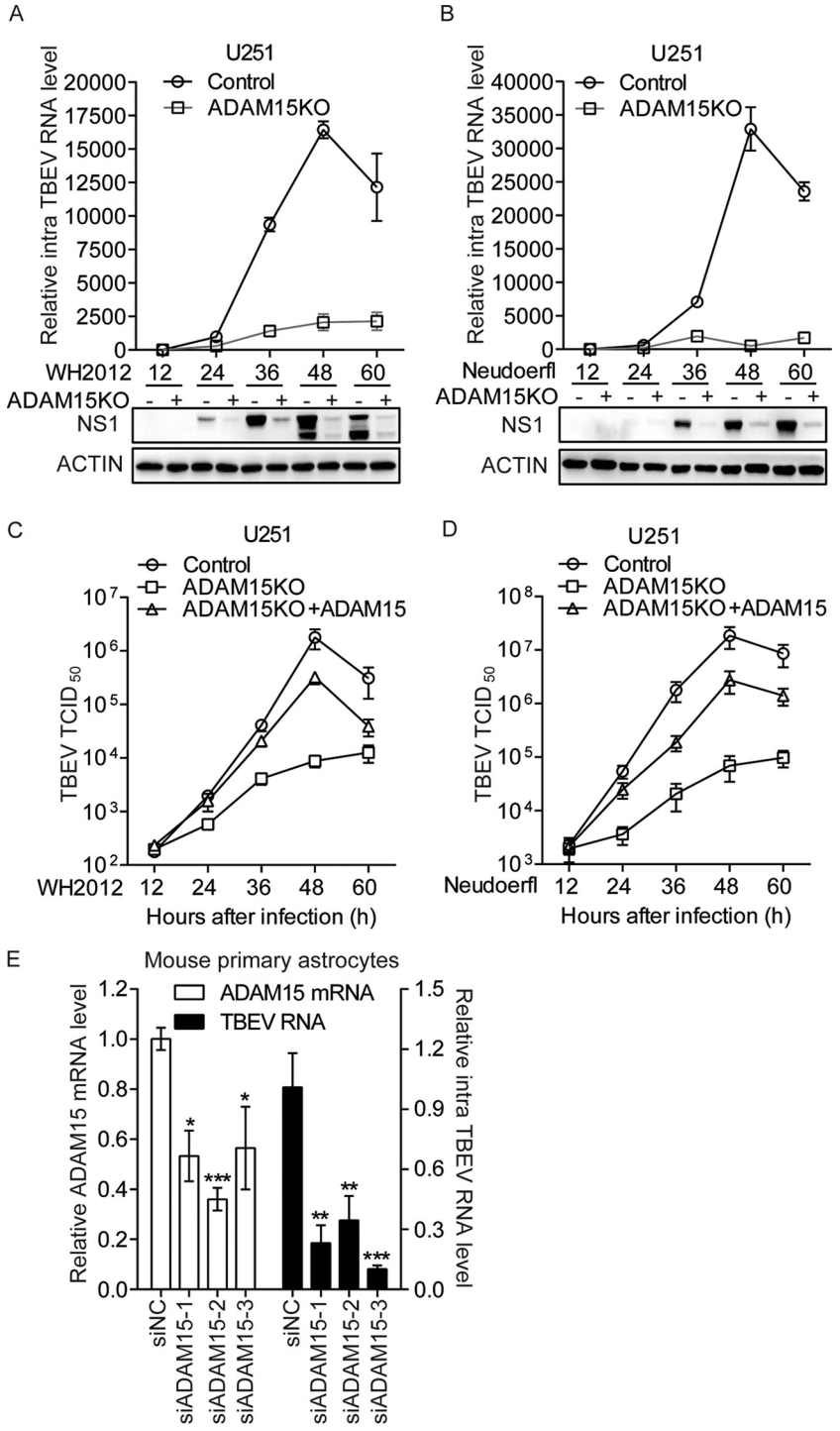

FIG 3 ADAM15 is required for optimal infection of TBEV. (A to D) Multistep growth curves with TBEV WH2012 (A and C) or TBEV Neudoerfl (B and D) in control, ADAM15$^{-/-}$, or ADAM15 transcomplemented ADAM15$^{-/-}$ U251 cells. (A and B) Mean change in intracellular viral RNA levels relative to the control cells. (C and D) Mean change in virus $TCID_{50}$ ml^{-1} relative to control cells. (E) Mouse primary astrocytes were transfected with siRNAs targeting ADAM15 mRNA transcripts or a nontargeting siRNA (control). At 48 h posttransfection, the intracellular ADAM15 mRNA and TBEV RNA levels were evaluated. Data are mean change relative to control cells and are representative of 3 independent experiments. Quantitative data are means and SD. *, $P < 0.05$; **, $P < 0.01$; ***, $P < 0.001$.

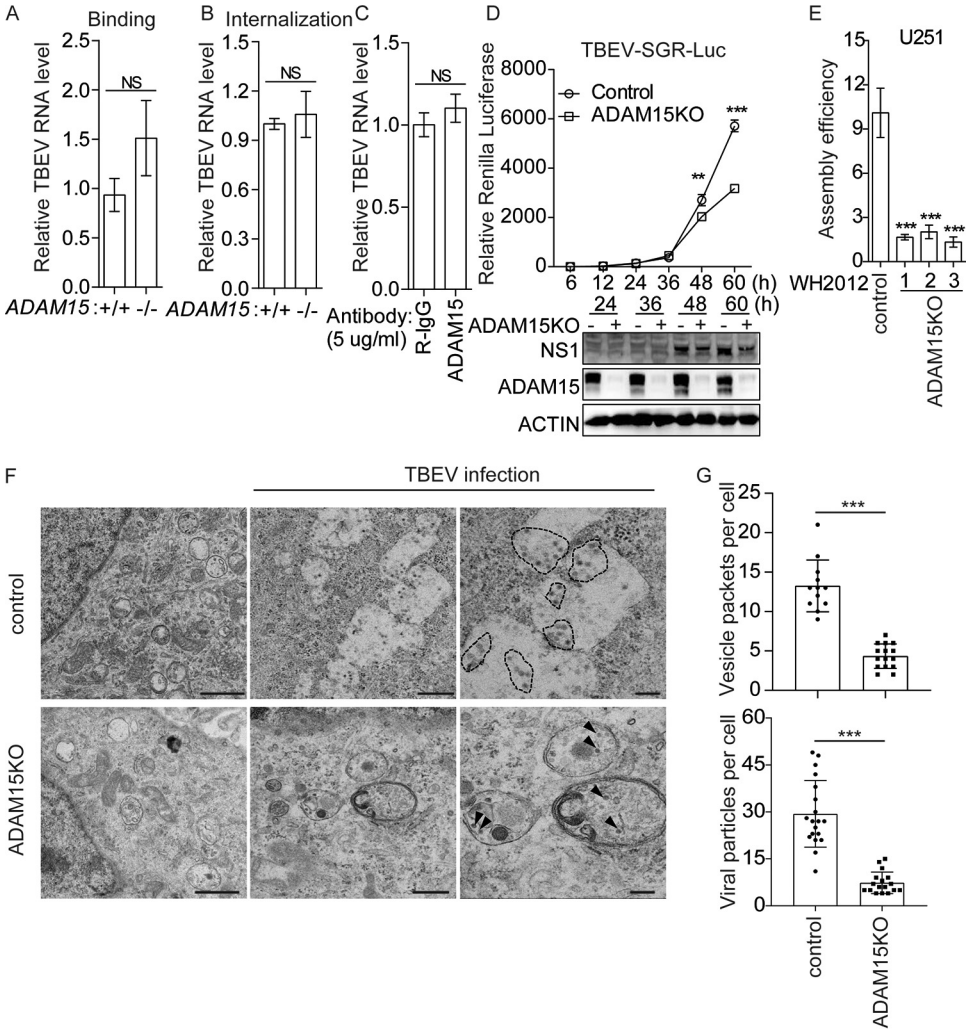

FIG 4 ADAM15 modulates TBEV replication and assembly. (A to C) Cells were collected and RNA was measured by qPCR/RT-PCR. Mean change in viral RNA levels relative to control cells is shown. (A and B) TBEV was incubated with control and ADAM15$^{-/-}$ cells at 4°C (A) or 37°C (B) as described in Materials and Methods. (C) Control and ADAM15$^{-/-}$ cells were incubated with anti-ADAM15 or isotype control MAbs before infection. (D) Transfection of TBEV subgenomic RNA into control or ADAM15$^{-/-}$ cells. Cells were analyzed for *Renilla* luciferase and NS1 protein expression levels. Mean change relative to control cells is shown. (E) Control and ADAM15$^{-/-}$ cells were infected with TBEV for 48 h, and then viral RNA levels in cells and culture supernatants were quantified. Mean change in assembly efficiency (RNA copies in supernatant/RNA copies in cells) relative to the control cells is shown. (F) After 48 h infection, cells were fixed with glutaraldehyde and processed for viewing by TEM. Mature particles (black arrowheads) are indicated. Bars, 1 μm (left), 500 nm (middle), and 200 nm (right). (G) Viral particles or vesicle packets were determined by counting using ImageJ software, and mean values are presented (error bars represent SD). Data are representative of 3 independent experiments. Quantitative data are means and SD. **, $P < 0.01$; ***, $P < 0.001$; NS, no significant difference.

ADAM15 mediates the TBEV RNA replication and virion assembly. To investigate the mechanism of ADAM15-mediated TBEV replication, the TBEV life cycle effect was evaluated in the *ADAM15* knockout cells. For TBEV entry, consistent with the experiments using anti-ADAM15 neutralizing antibodies, we observed no effect of the *ADAM15* knockout on TBEV RNA in cells RNA by binding and internalization assays (Fig. 4A to C). To determine whether ADAM15 is required for replication, we transfected TBEV subgenomic RNA into control and *ADAM15*$^{-/-}$ U251 cells, and lower TBEV RNA and NS1 protein levels were measured within *ADAM15*$^{-/-}$ cells (Fig. 4D). Next, we estimated the effect of *ADAM15* knockout on virion assembly. The knockout of *ADAM15* significantly reduced viral RNA levels in cells and culture supernatants. The ratios of supernatants and intracellular RNA copies were also reduced (Fig. 4E), suggesting that

ADAM15 affects virion assembly and/or release. These results indicated that ADAM15 supports TBEV infection and suggested that ADAM15 has different roles in viral RNA replication and assembly. We then examined the role of ADAM15 in TBEV infection using *in situ* transmission electron microscopy (TEM) to visualize possible changes in virus-induced ER and Golgi due to the *ADAM15* knockout. Consistent with previous studies (20), in control cells infected with TBEV, we observed the formation of vesicle packets and ER-wrapped virions (~40 nm in diameter) (Fig. 4F). In *ADAM15*$^{-/-}$ cells, vesicle size and shape were distorted, and fewer VPs were observed (Fig. 4F). Additionally, very few intracellular vesicle packets and viral particles were observed in *ADAM15*$^{-/-}$ cells (Fig. 4G). These results indicated that ADAM15 might be involved in the formation of vesicle packets induced by TBEV infection, which is important for genomic RNA replication.

TBEV infection alters ADAM15 subcellular localization. The experiments described above established that ADAM15 is closely related to the life cycle of TBEV. The next question was whether the expression or localization of ADAM15 changes during TBEV infection. Real-time PCR and Western blotting indicated no difference in ADAM15 mRNA or protein levels, suggesting that TBEV infection does not affect ADAM15 expression (Fig. 5A). The lysates of mock- or TBEV-infected control cells and ADAM15 knockout cells were subjected to membrane flotation fractionation. Caveolin-2 was used as a detergent-resistant-membrane (DRM)-positive control, and calnexin was used as a detergent-sensitive control (21). When the cell lysates were treated with 1% NP-40, a nonionic detergent, on ice, a condition which released the ER transmembrane protein calnexin to the cytosol, most of the TBEV NS1 protein was fractionated in the cytosol. However, in the presence of TBEV infection, the localization of ADAM15 was altered from the DRM to cytosol (Fig. 5B). Immunofluorescence showed that ADAM15 was enriched in ER and Golgi regions during TBEV infection compared to the uninfected group (Fig. 5C). Moreover, *ADAM15* knockout appeared to distort the ER and Golgi shapes (Fig. 5D). These results suggested that the TBEV infection could change the location of ADAM15.

Link between ADAM15 and the cellular endomembrane network. It was found that TBEV selectively exploits ADAM15. The virus infection might alter the location of ADAM15 and then change the formation of the membranous TBEV replication organelle. This observation should provide mechanistic insights. Therefore, we performed an RNA sequencing (RNA-Seq) analysis of wild-type (WT) and *ADAM15* knockdown U251 cells in the absence or presence of TBEV. When analyzing the difference in the expression of the same gene in two samples, we used two parameters: fold change, which reflects the difference multiplier of the same gene in different samples, and *P* value. The criteria for differentially expressed genes were a *P* value of <0.05 and a difference multiplier of more than 2. The fold change and *P* value data showed that there were 2,546 differentially expressed genes between no infection and TBEV infection. Compared with other comparison groups, analysis showed that a total of 1,198 differentially expressed genes were identified in TBEV infection in ADAM15 knockout cells and TBEV infection in WT cells. The comparison of the ADAM15 knockout cells and control cells found 507 differentially expressed genes. A Venn diagram showed that 38 common differentially expressed genes were identified in the above four comparison groups (Fig. 6A). Surprisingly, KEGG function analysis showed that various genes were less expressed in *ADAM15* knockdown cells than control cells. These genes function in the organization and formation of cellular membrane components and vesicles, as well as almost all pathways of relevance for flavivirus infection (Fig. 6B to D). TBEV was likely to hijack the specific cellular functions of ADAM15 to facilitate either replication through organelle biogenesis or virion assembly. Further study of these differentially expressed genes and pathways identified in our RNA-Seq analysis will provide important insights into ADAM15 function and its exploitation by TBEV.

ADAM15 differentially associates with viral proteins of TBEV. TBEV infection changes the location of ADAM15, and the function of ADAM15 is related to the organization and formation of cellular membrane components and vesicles. We speculated that the TBEV proteins could interact with ADAM15 to participate in the TBEV life cycle.

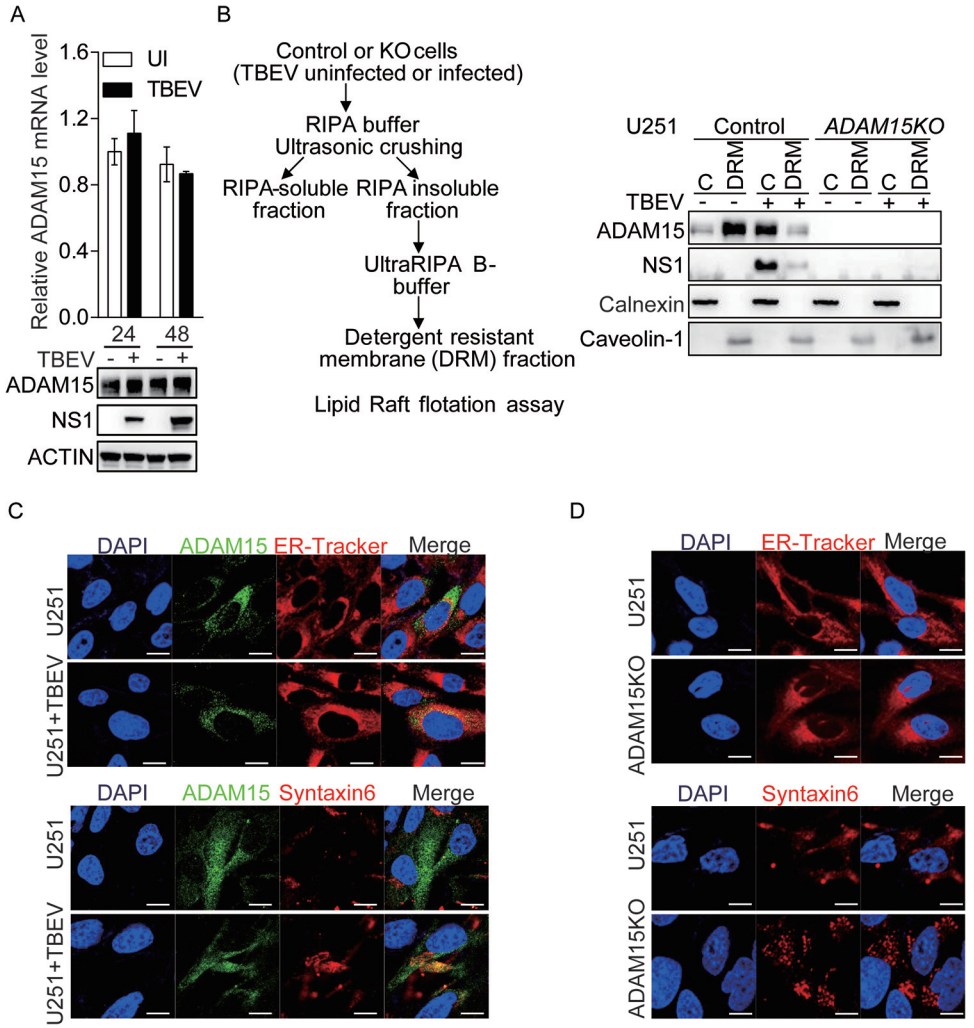

FIG 5 TBEV infection does not affect ADAM15 expression but changes the localization and distribution of ADAM15. Cells were infected with TBEV for the indicated times. (A) Mean change in ADAM15 mRNA and protein levels compared to uninfected cells. (B) After 48 h infection, lipid raft flotation analysis of ADAM15 localization in the RIPA-soluble fraction or DRM was carried out. Data are changes compared to uninfected cells. (C) After 48 h infection, cells were fixed with paraformaldehyde and stained for ADAM15, NS1, ER, or trans-Golgi. Cells were analyzed by confocal microscopy. Bar, 10 μm. (C and D) Control and ADAM15$^{-/-}$ cells were grown on glass dishes. Cells were fixed followed by staining for visualization and imaging by confocal microscopy. After 48 h infection, cells were fixed with paraformaldehyde and stained with ER tracker, endogenous ADAM15, or the Golgi marker syntaxin 6. Cells were then analyzed by confocal microscopy. Images were representative of 3 independent samples. Results are representative of 3 independent experiments. Quantitative data are means and SD.

To test the interaction between viral proteins and ADAM15, we performed coimmunoprecipitation (co-IP) experiments using hemagglutinin (HA)-tagged or enhanced green fluorescent protein (eGFP)-tagged ADAM15. ADAM15 associated with viral glycoproteins E, NS2A, and NS4B proteins (Fig. 7A to C). Consistent with the co-IP results, we found that fluorescent signals for ADAM15 were enriched in regions containing E, NS2A, and NS4B proteins (Fig. 7D). These results show the associations between ADAM15 and viral proteins, in particular E, NS2A, and NS4B proteins, which correlate with ADAM15's viral replication role during TBEV infection.

ADAM15 disintegrin domain is required for the TBEV replication cycle. The phenotypic differences among ADAMs in TBEV infection provided us with a unique opportunity to evaluate ADAM15-specific interaction with TBEV. To this end, we generated *ADAM15* deletion mutants to characterize subdomains responsible for unique functions (Fig. 8A). Domain mapping analysis indicated that the disintegrin domain (DD) of

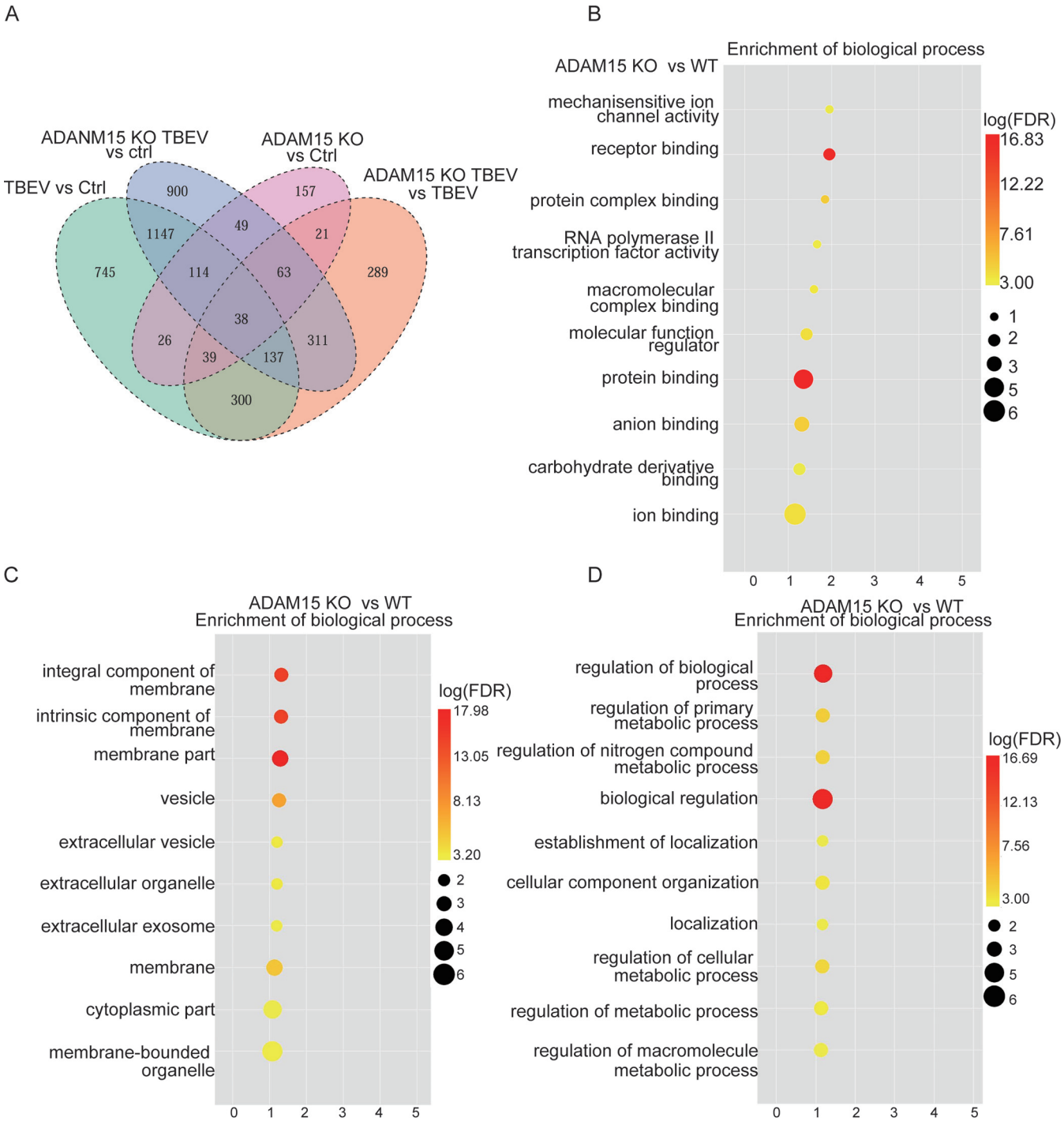

FIG 6 Differential gene KEGG function analysis. WT and ADAM15 knockdown U251 cells (three biological replicates in each group) were harvested 48 h after TBEV infection. Total cellular RNA was isolated, and whole-transcriptome sequencing was performed. (A) Venn diagram of four comparison groups of differentially expressed genes. (B to D) Functional analysis of differential gene KEGG functions. The *x* axis shows the enrichment score. The bigger the bubble, the more different genes it contains. The smaller the enrichment *P* value, the greater the significance.

ADAM15 (amino acids [aa] 420 to 510) is associated with E, NS2A, and NS4B (Fig. 8B to F). To determine if ADAM15's DD is required for the TBEV infection, we performed a transcomplementation in *ADAM15*$^{-/-}$ U251 cells. *ADAM15*$^{-/-}$ cells were transduced with constructs encoding the WT ADAM15 or DD, followed by infection with TBEV. WT ADAM15 and the DD (aa 420 to 510) and the C terminus of ADAM15 rescued virus replication (Fig. 8G). However, when the DD region was expressed in isolation from other

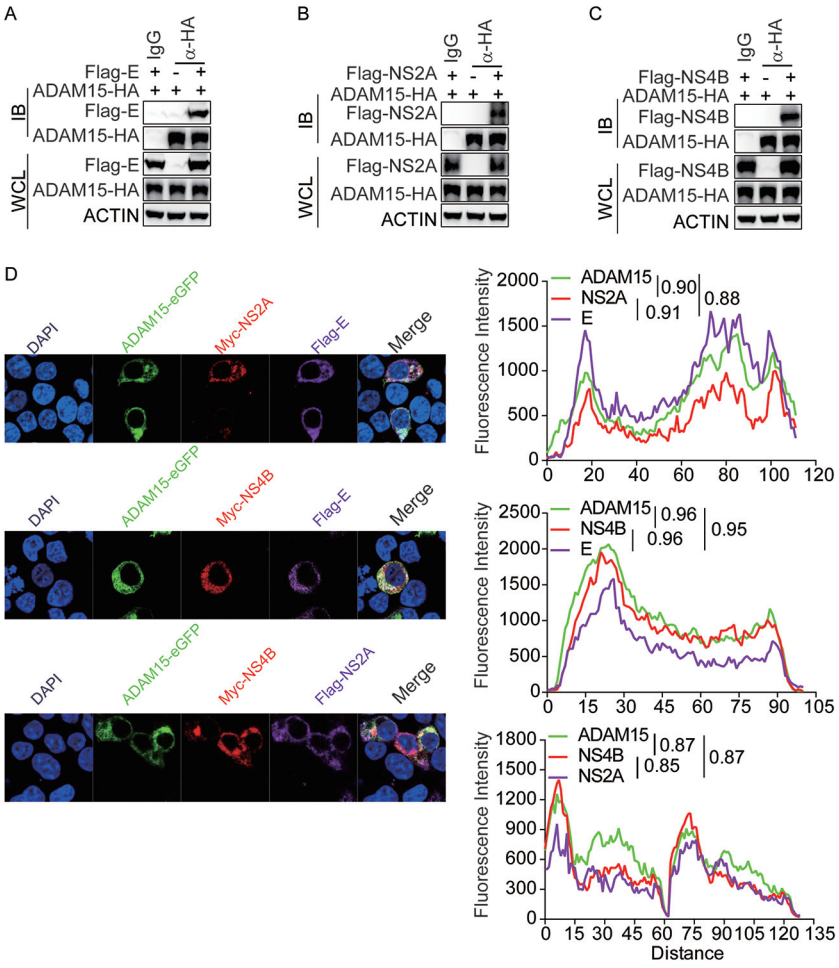

FIG 7 Mapping of functional domains of ADAM15 involved in the association with TBEV proteins. (A to C) HEK293T cells were transfected with Flag-E (A), Flag-NS2A (B), or Flag-NS4B (C) and ADAM15-HA plasmids for 48 h, respectively. Cells were lysed, and HA-tagged proteins were immunoprecipitated with anti-HA antibody. Inputs and precipitated proteins were determined by Western blotting for the indicated proteins. β-Actin served as the loading control. (D) HEK293T cells were transfected with various plasmids (ADAM15-eGFP, Myc-NS4B, Flag-E, or Flag-NS2) for 24 h. Cells were fixed with paraformaldehyde and stained using specific antibody. Cells were then analyzed by confocal microscopy. Fluorescence intensity and colocalization were determined using Volocity software. All results are representative of 3 independent experiments.

ADAM15 domains, it was not able to increase TBEV titers in ADAM15$^{-/-}$ cells (Fig. 8H). As shown in Fig. 8G and H, a possible reason is that DD isolation lacked a membrane anchor and dissociated the ER and Golgi (data not shown). We used ADAM15-420-C to rescue it and found that it can enhance virus titers. According to previous reports, the ADAM15 DD had important functions in integrin binding compared with other ADAMs (13). These results indicate nonredundant ADAM functions for ADAM15 in TBEV infection.

DISCUSSION

Previous studies demonstrated the involvement of TBEV infection in neuronal dysfunction and the development of neurological diseases (1, 10). In this study, we showed that the host factor ADAM15 supports TBEV replication and assembly processes, and we provide data for an integrated model of viral infection (Fig. 9). ADAM15 has been well characterized as a multifunctional disintegrin protease involved in cell adhesion, the degradation of extracellular matrix components, and ectodomain shedding of membrane-bound growth factors that are intrinsic to cancer and various

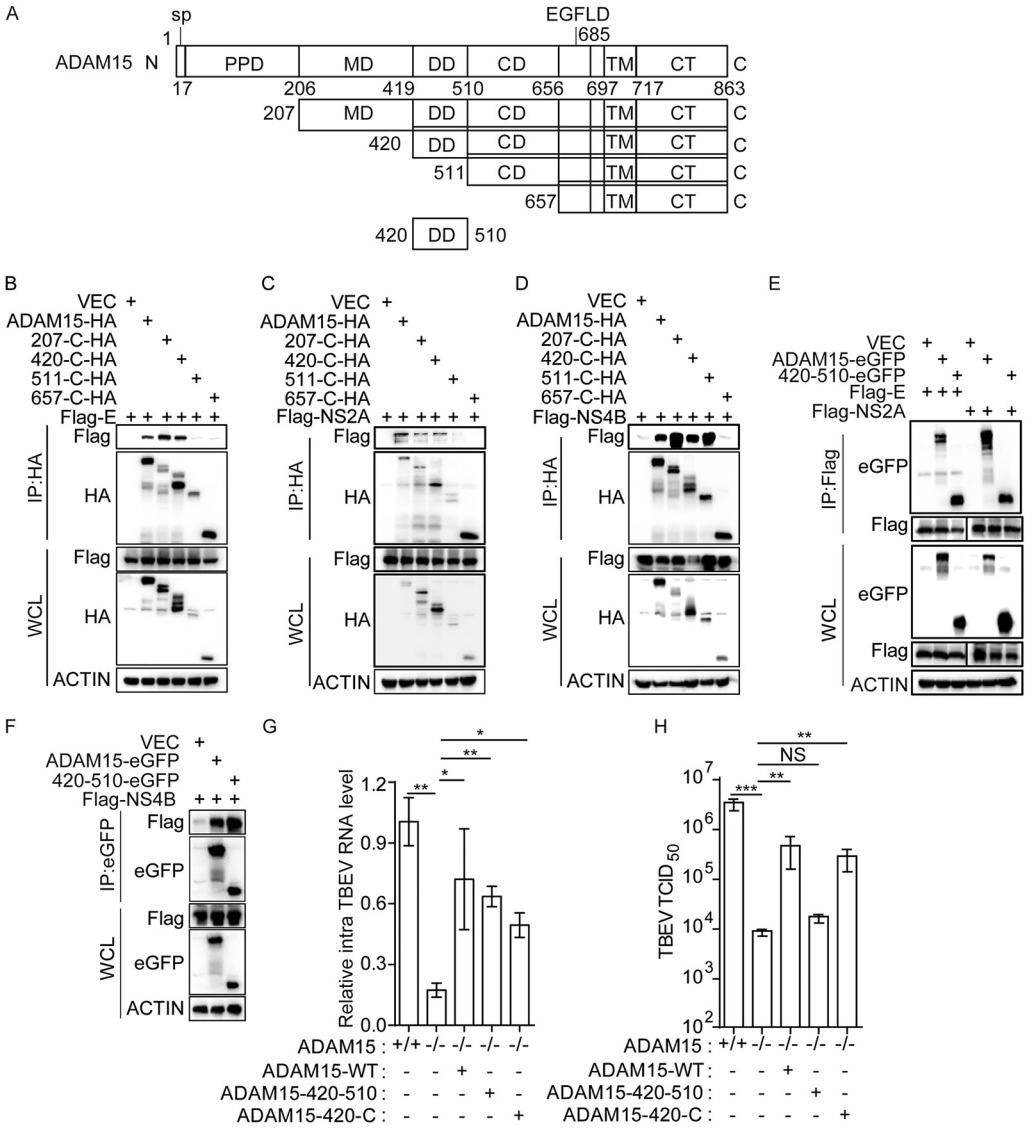

FIG 8 Mapping of functional domains of ADAM15 involved in the association with Flag-E, Flag-NS2A and Flag-NS4B. (A) Schematic representation of ADAM15 mutant constructs. ADAM15 was classified as a membrane-anchored ADAM containing propeptide domain (PPD), a metalloproteinase domain (MD), a disintegrin-like domain (DD), a cysteine-rich domain (CD), an epidermal growth factor-like domain (EGFLD), a transmembrane domain (TM), and a cytosolic tail (CT). (B to D) HEK293T cells were transfected with Flag-E (B), Flag-NS2A (C), or Flag-NS4B (D) and ADAM15 mutant constructs for 48 h. (E and F) HEK293T cells were transfected with Flag-NS2A (E) or Flag-NS4B (F) and ADAM15-eGFP or 420-510-eGFP plasmids for 24 h. Cells were lysed, and HA-tagged proteins were immunoprecipitated with anti-HA antibody. Inputs and precipitated proteins were determined by Western blotting for the indicated proteins. β-Actin served as a loading control. (G and H) TBEV WH2012 was used to infect naive cells, ADAM15$^{-/-}$ cells, ADAM15 transcomplemented ADAM15$^{-/-}$ cells, ADAM15-DD domain transcomplemented ADAM15$^{-/-}$ cells, or ADAM15-420-C transcomplemented ADAM15$^{-/-}$ U251 cells. The intracellular viral RNA (G) and virus titer (H) were quantified. Results are representative of 3 independent experiments. Quantitative data are means and SD. *, $P < 0.05$; **, $P < 0.01$; ***, $P < 0.001$; NS, no significant difference.

inflammatory conditions (22–26). ADAM15 is mainly expressed in neuroglia and endothelial cells in human brains, and TBEV infection can lead to injury of human astrocytes. Hence, ADAM15 appeared to have relevance for neurological diseases caused by TBEV infection. Consistent with our supposition, KEGG function analysis in *ADAM15* knockdown cells compared to control cells showed decreased expression for various genes related to the organization and formation of cellular membrane components and vesicles, as well as almost all pathways of relevance for virus

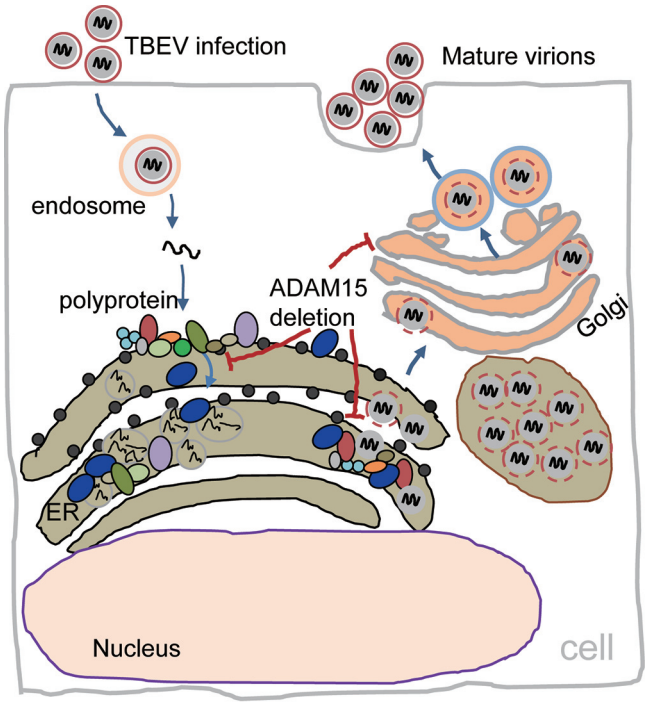

FIG 9 Model for the function of ADAM15 in TBEV infection.

infection (Fig. 6A to D). In particular, the ER membrane components are chosen by flaviviruses.

We focused on ADAM15 because it was the most strongly enriched candidate in the screen and scored with multiple orthologous siRNAs. Using a diverse panel of CRISPR-engineered *ADAM15* KO human cell lines, as well as *ADAM15* knockdown primary murine cell lines using *ADAM15* siRNA, we confirmed ADAM15's involvement in TBEV infection. We demonstrated that the loss of ADAM15 results in a profound block in the replication and assembly of TBEV infection. This study is the first to define a direct role for ADAM proteins in TBEV infection.

We identified a function for ADAM15 in TBEV replication and viral assembly (Fig. 4D to F). The viral RNA levels, NS1 protein levels, and viral titers were decreased in *ADAM15* knockdown or knockout cells compared to control cells (Fig. 2), as was the ratio of extracellular RNA copies to intracellular RNA copies (Fig. 4E). Consistently, multistep growth curves with TBEV infection were significantly reduced in ADAM15$^{-/-}$ cells compared to control cells (Fig. 3A to D). These data indicated that ADAM15 regulates TBEV replication and virion particle assembly.

Several studies had demonstrated that flavivirus NS4B created foci at the ER membrane, which were the sites of viral RNA synthesis (27–29). It had been reported the TBEV NS4B could interact with NS1, NS2A, NS2B, and NS4A to form viral replication compartments (RC) (29). Our observations suggested that these protein interactions taking place during RC formation were conserved among TBEV infections and that they could be reconstituted in our model system, which was consistent with previous data on other flaviviruses (30). Dilation of ER with replication vesicles had been observed in different cell lines infected with TBEV, including human neuronal cells, Caco-2 intestinal epithelial cells, and porcine stable kidney cells (29, 31–33). Dilation of the ER had been suggested to be linked to virion maturation and cytopathic effects of TBEV (34). Our results agreed with the suggestion that dilation of ER was important for virus replication and virion assembly. Additionally, we found a large proportion of ADAM15 localizing in the ER and Golgi during TBEV infection (Fig. 5C) and the overall number of intracellular virus particles accumulated in paracrystalline structures within

the lumen of ER cisternae (Fig. 5E). Furthermore, our TEM data showed a previously unidentified link between ADAM15 and virus-induced replication of organelles. It may be that ADAM15 contributes to contacting sites between ER tubules and Golgi and coordinates the interaction of virus replication and assembly. Further work must determine the precise function of ADAM15 in TBEV assembly.

The disintegrin domain of human ADAM15 contains an RGD integrin-binding motif. In addition, ADAM15 was upregulated at the surface of angiogenic endothelial cells (25). It has been reported that the DD of ADAM15 is associated with $\alpha v\beta 3$ and $\alpha 5\beta 1$ in an RGD-dependent manner (26). Moreover, we found that the DD of ADAM15 was sufficient to complement TBEV RNA replication (Fig. 8G) but not sufficient for TBEV virus production (Fig. 8H). The DD of ADAM15 had a slightly higher colocalization with E, NS2A, and NS4B proteins. This interaction might change the localization of ADAM15. Additional investigation on the structure-function relationship of the ADAM15 DD will provide useful information for understanding the physiological significance of ADAM15.

The description of this unique virus-host interaction improves our understanding of the molecular mechanisms of TBEV infection and pathogenicity. Our findings also increase the basic knowledge of the TBEV life cycle. This study will also promote the study of neurodegenerative diseases and highlights a target for pharmaceutical consideration due to its involvement in key TBEV infection processes.

MATERIALS AND METHODS

Cell lines and virus strains. U251 cells were obtained from the BeNa Culture Collection; BHK-21 (ATCC CCL10), Vero E6 (ATCC CRL-1586), HEK-293T (ATCC CRL-3216), and T98G (ATCC CRL-1690) cells were obtained from ATCC. U251, BHK-21, Vero E6, and HEK-293T cells were cultured in Dulbecco's modified Eagle medium (DMEM; Gibco), and T98G cells were cultured in minimum essential medium (MEM; ATCC) supplemented with 10% fetal bovine serum (FBS; Gibco), 100 U/ml of penicillin, and 100 μg/ml of streptomycin and maintained at 37°C in a fully humidified atmosphere containing 5% CO_2. The mouse primary astrocytes used in this study were isolated from fetal mice with the ICR background and maintained in astrocyte medium (ScienCell) supplemented with 10% FBS and 1% penicillin/streptomycin. All experiments with WT and ADAM15 knockout cell lines were performed within 20 cell passages. All cells were regularly tested for mycoplasma contamination and authenticated by visual observations of cell morphology.

TBEV Far Eastern subtype strain WH2012 (GenBank no. KJ755186) was obtained from the National Virus Resource Center, China. WH2012 stocks were prepared by virus amplification in BHK-21 cells. The infectious cDNA clones of TBEV European subtype prototypic strain Neudoerfl (GenBank no. U27495) were generously provided by F. X. Heinz at the Medical University of Vienna, Austria. Neudoerfl stocks were prepared by electroporation of BHK-21 cells with *in vitro*-transcribed Neudoerfl RNA and subsequent virus amplification in Vero E6 cells. The TBEV subgenomic replicon (kindly provided by Z. H. Zheng, Wuhan Institute of Virology, China) encodes *Renilla* luciferase. Quantification of TBEV RNA levels in cells and culture supernatants was done by quantitative PCR (qPCR) and reverse transcription PCR (RT-PCR). TBEV RNA replication was measured by *Renilla* luciferase assay. TBEV titers were determined by PFU assay in Vero E6 cells using an overlay medium containing 1.0% carboxymethylcellulose.

Reagents and antibodies. ER-Tracker red (C1041) and 4′,6-diamidino-2-phenylindole (DAPI) (C1002) were from Beyotime Biotechnology (China). The following antibodies were used for Western blotting or immunoprecipitation: anti-Flag (catalog no. F1804; Sigma), anti-GFP (catalog no. MA5-15256; Invitrogen), anti-HA (catalog no. H9658; Sigma), anti-caveolin-1 (catalog no. 3267; Cell Signaling Technology), anti-calnexin (catalog no. 2679; Cell Signaling Technology), anti-ADAM15 (catalog no. ab124698 and ab137387; Abcam), and anti-beta-actin (catalog no. 66009-1-Ig; Proteintech). The antibody against NS1 of TBEV was custom produced by Abmart (Shanghai, China). The proteins were visualized using suitable horseradish peroxidase (HRP)-conjugated secondary antibodies (Jackson ImmunoResearch) and SuperSignal-Femto chemiluminescent substrate (Pierce).

Expression constructs and transfection. ADAM15 and ADAM15 truncations with an HA tag or an eGFP tag at the C terminus were cloned into pcDNA3.1(−) vector. The lentivirus expression plasmid pLVX-puro-ADAM15 was purchased from Tsingke (China). Flag-tagged TBEV C, prM, E, NS1, NS2A, NS2B, NS3, NS4A, NS4B, and NS5 expression constructs were kindly provided by Q. X. Hu at Wuhan Institute of Virology, Chinese Academy of Science. The plasmids transfection was performed using Lipofectamine 3000 (Invitrogen) transfection reagent according to the manufacturer's protocol.

Lentivirus production and titration. Delivery of expression plasmids for knockout or overexpression experiments was done through transduction with lentiviruses. For preparation of lentiviruses stocks, HEK-293T cells in T25 flasks were transfected at ~90% confluence with packaging plasmids psPAX2 (2,250 ng; Addgene) and pMD2.G (750 ng; Addgene) and specific plasmids (3,000 ng) expressing sgRNA or ADAM15. Approximately 60 h after transfection, the cell medium containing the lentivirus was harvested and filtered through a 0.45-μm filter. Lentiviruses were titrated in a SYBR green I-based real-time

PCR-enhanced reverse transcriptase (SG-PERT) assay (35). For all experiments, transductions were performed in the presence of 10 μg ml^{-1} Polybrene.

RNAi experiments. The sequences of siRNAs specific for ADAM15 were purchased from GenePharma. The sequences were as follows: ADAM8, 5′-GGAUGGCACUGCGUAUGAATT-3′ and 5′-UUCAUACGCAGUGCCAUCCTT-3′; ADAM9, 5′-CUCCCUCCUGUGGUAAUATT-3′ and 5′-UAUUACCA CAGGAGGGAGCTT-3′; ADAM10, 5-GCUAAUGGCUGGAUUUAUUTT-3′ and 5′-AAUAAAUCCAGCCAUUAGCTT-3′; ADAM11, 5′-CCAAGUAUGUGGAGCUAAUTT-3′ and 5′-AUUAGCUCCACAUACUUGGTT-3′; ADAM12, 5′-GCCGUUUCCAUAGAAACAATT-3′ and 5′-UUGUUUCUAUGGAAACGGCTT-3′; ADAM15-1, 5′-GCUGCUUUCU GCGGAAAUATT-3′ and 5′-UAUUUCCGCAGAAAGCAGCTT-3′; ADAM15-2, 5′-GGGAGACAAUAGAUGUGAATT-3′ and 5′-UUCACAUCUAUUGUCUCCCTT-3′; ADAM15-3, 5′-GCACAGGAAUGUCGAAGCATT-3′ and 5′-UGCUUCGACAUUCCUGUGCTT-3′; ADAM17, 5′-GAUCAUCGCUUCUACAGAUTT-3′ and 5′-AUCUGUAGAAGC GAUGAUCTT-3′; ADAM19, 5′-GCUACAACCAUAUUUGCUUTT-3′ and 5′-AAGCAAAUAUGGUUGUAGCTT-3′; ADAM22, 5′-GCUUCCAGGUUGAUGCCUUTT-3′ and 5′-AAGGCAUCAACCUGGAAGCTT-3′; mouse ADAM15-1, 5′-CCUGAGGCCCUGAGGAUUUTT-3′ and 5′-AAAUCCUCAGGGCCUCAGGTT-3′; mouse ADAM15-2, 5′-GGAGCACAGGAAUGUCGAATT-3′ and 5′-UUCGACAUUCCUGUGCUCCTT-3′; mouse ADAM15-3, 5′-GGGCACCUCCAGACUGCAUTT-3′ and 5′-AUGCAGUCUGGAGGUGCCCTT-3′. The siRNAs were transfected using Lipofectamine RNAiMAX reagent (Invitrogen) at a final concentration of 20 nM according to the manufacturer's instructions. To keep ADAM15 silencing efficiency for the duration of the test, the cells were split at 24 h posttransfection and transfected with the same siRNA again. TBEV infection assay was performed 24 h after the second transfection.

CRISPR-Cas9-mediated ADAM15 knockout and ADAM15 rescue experiments. The 20-base single-guide RNAs (sgRNA) used to target ADAM15 were as follows: ADAM15KO-1, 5′-TAATTGGGAGATCGTCCTGA-3′ and 5′-TCAGGACGATCTCCCAATTA-3′; ADAM15KO-2, 5′-ACTGACCACC CGAGTGCCAT-3′ and 5′-ATGGCACTCGGGTGGTCAGT-3′; ADAM15KO-3, 5′-AGCTCCAACTTGATCCTCAG-3′ and 5′-CTGAGGATCAAGTTGGAGCT-3′. CRISPR plasmids were constructed by insertion of the annealed oligonucleotides into the lentiCRISPRv2 plasmids (Addgene) encoding puromycin or GFP for ADAM15. To generate stable cell lines, T98G and U251 cells at ~50% confluence were infected with the respective lentivirus at a multiplicity of infection (MOI) of 0.3 and 24 h later the cells were cultured in medium containing 2 μg ml^{-1} puromycin for 10 days. The resulting knockout efficiency was analyzed using Western blotting assays and Sanger DNA sequencing. ADAM15 knockout monoclonal cells were sorted by flow cytometry (using a flow cytometer from BD Bioscience) for the loss of ADAM15 expression.

For the rescue experiments, ADAM15$^{-/-}$ cells were plated at 1×10^5 cells per well in 24-well plates and transduced with the specified lentivirus particles (MOI = 5). At 72 h after transduction, cells were infected with TBEV at an MOI of 0.5, TBEV RNA levels in cells were determined by qPCR/RT-PCR, and cell culture supernatants were evaluated for virus titer using a PFU assay.

Cell viability assay. Cell viability of transfected or transduced cells was evaluated using a CellTiter-Glo luminescent cell viability assay kit (Promega) according to the manufacturer's instructions. In brief, 1×10^4 cells in 100 μl culture medium were seeded into opaque-walled 96-well plates. After 24 h, 100 μl of CellTiter-Glo reagent was added to each well and subjected to shaking for 5 min. After 10 min incubation at room temperature, luminescence was recorded by using a GloMax 20/20 luminometer (Turner BioSystems). Three independent experiments, each in triplicate, were performed, and results of one representative experiment are shown.

Virus binding and internalization assays. Control or ADAM15$^{-/-}$ cells were washed twice with ice-cold phosphate-buffered saline (PBS) and incubated with TBEV at an MOI of 20 in cold medium supplemented with 2% FBS DMEM on ice for 1 h. For the binding assay, the supernatant was then removed and the cells were washed five times with cold PBS. After the washes, cells were collected and RNA was measured by qPCR/RT-PCR. For the internalization assay, after five washes, cells were incubated using medium supplemented with 2% FBS and 15 mM NH_4Cl and then incubated at 37°C for 1 h. Cells were chilled on ice and treated with 500 ng/ml proteinase K on ice for 1 h. After three additional washes, cells were collected and RNA was measured by qPCR/RT-PCR.

Blocking assays with anti-ADAM15 MAbs. U251 cells (1×10^5) were seeded into 24-well plates 16 h before treatment. Cells were preincubated with isotype control or ADAM15 monoclonal antibodies (MAbs) for 1 h at 37°C in a volume of 100 μl, and then virions (MOI of 1) were added and incubated for 16 h. After three washes, cells were collected and RNA was measured by qPCR/RT-PCR.

qPCR/RT-PCR. Total cellular RNA was isolated with TRIzol (Invitrogen) reagent according to the manufacturer's protocols. Viral RNA in culture supernatants was extracted using a QIAamp viral RNA minikit (Qiagen) according to the manufacturer's instructions. The specific gene transcripts were quantified by one-step real-time qPCR/RT-PCR with the HiScript II One Step qRT-PCR SYBR green kit (Vazyme) using specific primers and the Applied Biosystems QuantStudio 6 Flex PCR system. The primer sequences for qPCR/RT-PCR (forward and reverse) were as follows: ADAM8 (human), 5′-CAGACCTGCACCTGATCGAG-3′ and 5′-CATTGTCCACGACCACATACA-3′; ADAM9 (human), 5′-GCTAGTTGGACTGGAGATTTGG-3′ and 5′-GTGGCTCCTTGAACACACTG-3′; ADAM10 (human), 5′-GGAGTGTACGTGTGCCAGTTCTG-3′ and 5′-GGTTCGACCACTGAAGTGCCTAC-3′; ADAM11 (human), 5′-GATGGGAACTTGACTTACATCGT-3′ and 5′-TCCGGTAAATGAGGTGGGGA-3′; ADAM12 (human), 5′-AACCTCGCTGCAAAGAATGTG-3′ and 5′-CTCTGAAACTCTCGGTTGTCTG-3′; ADAM15 (human), 5′-CACACTCAGAAGCCACCAGAGC-3′ and 5′-ATCAGCCACAATCACCAACTCCAC-3′; ADAM17 (human), 5′-GACTCTAGGGTTCTAGCCCAC-3′ and 5′-GGAGACTGCAAACGTGAAACAT-3′; ADAM19 (human), 5′-ACCCTCAAACCACCACACG-3′ and 5′-GCTCACCGTAATCAGTCCTCTA-3′; ADAM22 (human), 5′-GGGCCATATCCGAGGAAACC-3′ and 5′-TTCCCGTCATAGAACATCCCA-3′; ADAM15 (mouse), 5′-CCGCCGCTGCCAAATATAG-3′ and 5′-GGC CTCAGGTAAACCAGTCTG-3′; TBEV (WH2012), 5′-CACAACCTGGAGTGCTCG-3′ and 5′-ACCATGTT

CGGCCTTATC-3′; TBEV (Neudoerfl), 5′-GCAGCCAGATGCCCAACAATGG-3′ and 5′-TCTTTTTTGCC TCACAAGCCGCCT-3′; β-actin (human), 5′-CTCGACACCAGGGCGTTATG-3′ and 5′-CCACTCCATGC TCGATAGGAT-3′; actin (mouse), 5′-AGTGTGACGTTGACATCCGT-3′ and 5′-GCAGCTCAGTAACAG TCCGC-3′. The data were normalized to levels of β-actin mRNA in each individual sample. For all experiments, the $2^{-\Delta\Delta CT}$ method and standard curve line were used to calculate relative expression changes and absolute quantification, respectively.

Western blotting and coimmunoprecipitation. Whole-cell lysates for both Western blotting (WB) and co-IP were prepared using a lysis buffer containing 50 mM Tris-base (pH 7.5), 1 mM EGTA, 1 mM EDTA, 1% Triton X-100, 150 mM NaCl, 100 μM phenylmethylsulfonyl fluoride (PMSF), and protease inhibitors (Roche) for 30 min in 4°C. Cell lysates were centrifuged at 14,000 $\times$ *g* for 10 min at 4°C and quantified using the Bradford method. For WB, the supernatants were recovered, followed by denaturation at 95°C for 10 min. For co-IP, the supernatants were collected and mixed with protein G-agarose (Millipore) and various antibodies for 16 h at 4°C. Protein G-agarose-bound immune complexes were then eluted and subjected to WB analysis.

A 30-μg portion of total protein from each sample was resolved by SDS-PAGE and transferred to nitrocellulose. Membranes were blocked with Tris-buffered saline (pH 7.4) with 0.1% Tween 20 (TBST) containing 5% skim milk for 1 h at room temperature, followed by incubation with antisera containing primary antibodies overnight at 4°C. Membranes were washed and incubated for 1 h at room temperature with the HRP-conjugated secondary antibodies. Membranes were imaged using the FluorChem HD2 system (Alpha Innotech). Images were analyzed using AlphaEaseFC software (Alpha Innotech).

Immunofluorescent confocal microscopy. All cells were grown on glass dishes. HEK293T cells were transfected with the indicated plasmids by Lipofectamine 3000. WT and *ADAM15*$^{-/-}$ U251 cells were infected with TBEV at an MOI of 0.5. At 24 h after transfection or infection, the cells were fixed with 3.7% paraformaldehyde (PFA) at room temperature for 20 min and permeabilized in 0.5% Triton X-100 for 10 min at 4°C. Coverslips were blocked in 1% normal goat serum (AR1009; Boster) in PBS for 1 h and incubated with the indicated primary antibodies (anti-ADAM15 or anti-Syntaxin6 in Fig. 5C and D; anti-Myc or anti-Flag in Fig. 7D) at 4°C overnight. Samples were washed with PBS and incubated with secondary antibodies for 60 min at 37°C. Samples were then washed with PBS and stained with DAPI, followed by observation of glass coverslips using a Perkin Elmer UltraView Vox confocal microscope under a 60$\times$ oil objective.

Lipid raft flotation. WT and ADAM15$^{-/-}$ U251 cells were infected with TBEV at an MOI of 0.5. At 48 h after infection, culture supernatants were removed and cells were washed with PBS, followed by lysing in radioimmunoprecipitation assay (RIPA) lysis buffer (50 mM Tris [pH 8], 150 mM NaCl, 0.1% SDS, 0.5% sodium deoxycholate, 1% Triton X-100, 1$\times$ protease inhibitor cocktail, and 1 mM PMSF) by pipetting and incubating for 10 min on ice. Samples were centrifuged at 18,000 $\times$ *g* for 5 min at 4°C and the supernatants were transferred to another tube as the RIPA buffer-soluble fraction. The pellet was lysed by vigorous resuspension in UltraRIPA lysis buffer (F015; Diagnocine) with pipetting and incubation for 5 min at room temperature. Lysates were clarified by centrifugation at 18,000 $\times$ *g* for 5 min at room temperature. The supernatants were transferred to another tube as the lipid raft membrane fraction (also called the detergent-resistant membrane [DRM] fraction).

***In situ* transmission electron microscopy.** Cells grown on 6-well plates were fixed for 4 h by incubation with 2.5% glutaraldehyde at room temperature. After 3 washes with 0.1 M PBS (pH 7.4), cells were incubated with 1% osmium in 0.1 M PBS (pH 7.4) for 20 min and washed with 0.1 M PBS (pH 7.4) 3 times. Cells were progressively dehydrated with increasing concentrations of ethanol (30%, 50%, 70%, 80%, 85%, 90%, 95%, and 100%) and infiltrated with acetone-epoxy (1:1) for 3 h at 37°C, followed by infiltration in epoxy for 3 h at 37°C. Finally, cells were infiltrated with polymerizing Epon/Araldite resin (Araldite 502/EMbed 812 kit; Electron Microscopy Sciences) for 72 h at 60°C. Embedded cells were sectioned into 80-nm-thick slices by using an Ultracut UCT microtome (Leica) and a diamond knife (Diatome). After counterstaining with 2% uranyl acetate and 2% lead citrate in water for 15 min, cells were examined with a Tecnai G^2 20 Twin transmission electron microscope. Quantification of virion number, size, and distribution was done manually.

RNA sequencing analysis. WT and ADAM15 knockdown U251 cells (three biological replicates in each group) were harvested 48 h after infection. Whole-transcriptome sequencing was performed by Tsingke Biotechnology Inc. (Beijing, China). RNA-Seq short reads were aligned to the human genome (GRCh38) using GSNAP (36). Gene expression was counted as the number of short reads fully or partially aligned to the annotated gene model using Htseq (37). Differentially expressed genes (DEGs) were identified using the R Bioconductor package edgeR (38). *P* values were adjusted for multiple testing using false discovery rates (FDRs) (39). Significant DEGs were identified with an FDR of $\leq$0.05 and a $\log_2$ (fold change) of $\geq$1. Gene Ontology (GO) enrichment analysis was performed using Gorilla (40) by comparing the up- and downregulated DEGs to a list of all expressed genes. Significant GO terms with FDRs of $\leq$0.05 were reported. For original data, see Data Set S1.

Statistical analyses. The data are presented as means and standard deviations (SD). Significant differences between groups were determined using Student's *t* test or analysis of variance (ANOVA) as indicated, with 95% confidence intervals. The results of qPCR/RT-PCR or RNA-Seq were converted into β-actin expression to allow the relative gene expression of each sample to be presented within the same set of data. Unless otherwise stated, all qPCR/RT-PCR, WB, immunofluorescence, and microscopy images shown in this study are representative of at least 3 biological replicates.

Supporting data. Data Set S1 provides data for the CRISPR-Cas9 screen and gene analysis. The remainder of the data that support the findings of this study are available from the corresponding authors upon request.

SUPPLEMENTAL MATERIAL

Supplemental material is available online only.

SUPPLEMENTAL FILE 1, XLSX file, 7.8 MB.

ACKNOWLEDGMENTS

We thank the National Virus Resource Center (NVRC, China) for provision of TBEV Far-Eastern subtype strain WH2012. We thank F. X. Heinz for providing the infectious cDNA clones of TBEV European subtype prototypic strain Neudoerfl. We thank Q. X. Hu and Z. Q. Cui for providing the expression plasmids of TBEV. We thank Z. H. Zheng for providing the TBEV subgenomic replicon. We acknowledge the Core Facility Center of Wuhan Institute of Virology for continuous and generous support. We also thank D. Gao, A. N. Du, L. Zhang, J. Min, and P. Zhang for excellent technical support.

This study was supported by the National Key Research and Development Program of China (2018YFA0507201 to X.C. and 2018YFA0507202 to Y.Z.), the Youth Fund of National Natural Science Foundation of China (32000111 to Q.Y.), and the Program for Youth Innovation Promotion Association in Chinese Academy of Science to J.C.

We declare no competing interests.

Q. Yang and J. Chen designed the concept of the project, carried out the majority of the experiments, interpreted the results, and wrote the manuscript. Y. Zhou provided reagents and advice for the experiments. R. Pei and Y. Wang contributed to the critical discussions. J. Chen and X. Chen contributed to the concept of the study.

REFERENCES

1. Lindquist L, Vapalahti O. 2008. Tick-borne encephalitis. Lancet 371:1861–1871. https://doi.org/10.1016/S0140-6736(08)60800-4.
2. Suss J. 2011. Tick-borne encephalitis 2010: epidemiology, risk areas, and virus strains in Europe and Asia-an overview. Ticks Tick Borne Dis 2:2–15. https://doi.org/10.1016/j.ttbdis.2010.10.007.
3. Karbowiak G, Biernat B. 2016. The role of particular tick developmental stages in the circulation of tick-borne pathogens affecting humans in Central Europe. 2. Tick-borne encephalitis virus. Ann Parasitol 62:3–9. https://doi.org/10.17420/ap6201.25.
4. Mihalca AD, Sandor AD. 2013. The role of rodents in the ecology of Ixodes ricinus and associated pathogens in Central and Eastern Europe. Front Cell Infect Microbiol 3:56. https://doi.org/10.3389/fcimb.2013.00056.
5. Dobler G, Gniel D, Petermann R, Pfeffer M. 2012. Epidemiology and distribution of tick-borne encephalitis. Wien Med Wochenschr 162:230–238. https://doi.org/10.1007/s10354-012-0100-5.
6. Füzik T, Formanová P, Růžek D, Yoshii K, Niedrig M, Plevka P. 2018. Structure of tick-borne encephalitis virus and its neutralization by a monoclonal antibody. Nat Commun 9:436. https://doi.org/10.1038/s41467-018-02882-0.
7. Dai X, Shang G, Lu S, Yang J, Xu J. 2018. A new subtype of eastern tick-borne encephalitis virus discovered in Qinghai-Tibet Plateau, China. Emerg Microbes Infect 7:74. https://doi.org/10.1038/s41426-018-0081-6.
8. Tkachev SE, Babkin IV, Chicherina GS, Kozlova IV, Verkhozina MM, Demina TV, Lisak OV, Doroshchenko EK, Dzhioev YP, Suntsova OV, Belokopytova PS, Tikunov AY, Savinova YS, Paramonov AI, Glupov VV, Zlobin VI, Tikunova NV. 2020. Genetic diversity and geographical distribution of the Siberian subtype of the tick-borne encephalitis virus. Ticks Tick Borne Dis 11:101327. https://doi.org/10.1016/j.ttbdis.2019.101327.
9. Taba P, Schmutzhard E, Forsberg P, Lutsar I, Ljostad U, Mygland A, Levchenko I, Strle F, Steiner I. 2017. EAN consensus review on prevention, diagnosis and management of tick-borne encephalitis. Eur J Neurol 24:1214–e1261. https://doi.org/10.1111/ene.13356.
10. Hirano M, Muto M, Sakai M, Kondo H, Kobayashi S, Kariwa H, Yoshii K. 2017. Dendritic transport of tick-borne flavivirus RNA by neuronal granules affects development of neurological disease. Proc Natl Acad Sci U S A 114:9960–9965. https://doi.org/10.1073/pnas.1704454114.
11. Murphy G. 2008. The ADAMs: signalling scissors in the tumour microenvironment. Nat Rev Cancer 8:929–941. https://doi.org/10.1038/nrc2459.
12. Blobel CP. 2005. ADAMs: key components in EGFR signalling and development. Nat Rev Mol Cell Biol 6:32–43. https://doi.org/10.1038/nrm1548.
13. Lucas N, Najy AJ, Day ML. 2009. The therapeutic potential of ADAM15. Curr Pharm Des 15:2311–2318. https://doi.org/10.2174/138161209788682370.
14. Edwards DR, Handsley MM, Pennington CJ. 2008. The ADAM metalloproteinases. Mol Aspects Med 29:258–289. https://doi.org/10.1016/j.mam.2008.08.001.
15. Lindqvist R, Mundt F, Gilthorpe JD, Wolfel S, Gekara NO, Kroger A, Overby AK. 2016. Fast type I interferon response protects astrocytes from flavivirus infection and virus-induced cytopathic effects. J Neuroinflammation 13:277. https://doi.org/10.1186/s12974-016-0748-7.
16. Palus M, Bílý T, Elsterová J, Langhansová H, Salát J, Vancová M, Růžek D. 2014. Infection and injury of human astrocytes by tick-borne encephalitis virus. J Gen Virol 95:2411–2426. https://doi.org/10.1099/vir.0.068411-0.
17. Lee JH, Ostalecki C, Zhao Z, Kesti T, Bruns H, Simon B, Harrer T, Saksela K, Baur AS. 2018. HIV activates the tyrosine iinase Hck to secrete ADAM protease-containing extracellular vesicles. EBioMedicine 28:151–161. https://doi.org/10.1016/j.ebiom.2018.01.004.
18. Kim D, Ko HS, Park GB, Hur DY, Kim YS, Yang JW. 2017. Vandetanib and ADAM inhibitors synergistically attenuate the pathological migration of EBV-infected retinal pigment epithelial cells by regulating the VEGF-mediated MAPK pathway. Exp Ther Med 13:1415–1425. https://doi.org/10.3892/etm.2017.4110.
19. Bazzone LE, King M, MacKay CR, Kyawe PP, Meraner P, Lindstrom D, Rojas-Quintero J, Owen CA, Wang JP, Brass AL, Kurt-Jones EA, Finberg RW. 2019. A disintegrin and metalloproteinase 9 domain (ADAM9) is a major susceptibility factor in the early stages of encephalomyocarditis virus Infection. mBio 10:e02734-18. https://doi.org/10.1128/mBio.02734-18.
20. Miorin L, Maiuri P, Hoenninger VM, Mandl CW, Marcello A. 2008. Spatial and temporal organization of tick-borne encephalitis flavivirus replicated RNA in living cells. Virology 379:64–77. https://doi.org/10.1016/j.virol.2008.06.025.
21. Aizaki H, Lee KJ, Sung VM, Ishiko H, Lai MM. 2004. Characterization of the hepatitis C virus RNA replication complex associated with lipid rafts. Virology 324:450–461. https://doi.org/10.1016/j.virol.2004.03.034.
22. Bohm BB, Aigner T, Roy B, Brodie TA, Blobel CP, Burkhardt H. 2005. Homeostatic effects of the metalloproteinase disintegrin ADAM15 in degenerative cartilage remodeling. Arthritis Rheum 52:1100–1109. https://doi.org/10.1002/art.20974.
23. Fourie AM, Coles F, Moreno V, Karlsson L. 2003. Catalytic activity of ADAM8, ADAM15, and MDC-L (ADAM28) on synthetic peptide substrates and in ectodomain cleavage of CD23. J Biol Chem 278:30469–30477. https://doi.org/10.1074/jbc.M213157200.
24. Najy AJ, Day KC, Day ML. 2008. The ectodomain shedding of E-cadherin

by ADAM15 supports ErbB receptor activation. J Biol Chem 283:18393–18401. https://doi.org/10.1074/jbc.M801329200.
25. Horiuchi K, Weskamp G, Lum L, Hammes HP, Cai H, Brodie TA, Ludwig T, Chiusaroli R, Baron R, Preissner KT, Manova K, Blobel CP. 2003. Potential role for ADAM15 in pathological neovascularization in mice. Mol Cell Biol 23:5614–5624. https://doi.org/10.1128/mcb.23.16.5614-5624.2003.
26. Kuefer R, Day KC, Kleer CG, Sabel MS, Hofer MD, Varambally S, Zorn CS, Chinnaiyan AM, Rubin MA, Day ML. 2006. ADAM15 disintegrin is associated with aggressive prostate and breast cancer disease. Neoplasia 8:319–329. https://doi.org/10.1593/neo.05682.
27. Overby AK, Popov VL, Niedrig M, Weber F. 2010. Tick-borne encephalitis virus delays interferon induction and hides its double-stranded RNA in intracellular membrane vesicles. J Virol 84:8470–8483. https://doi.org/10.1128/JVI.00176-10.
28. El-Hage N, Luo G. 2003. Replication of hepatitis C virus RNA occurs in a membrane-bound replication complex containing nonstructural viral proteins and RNA. J Gen Virol 84:2761–2769. https://doi.org/10.1099/vir.0.19305-0.
29. Yau WL, Nguyen-Dinh V, Larsson E, Lindqvist R, Overby AK, Lundmark R. 2019. Model system for the formation of tick-borne encephalitis virus replication compartments without viral RNA replication. J Virol 93:e00292-19. https://doi.org/10.1128/JVI.00292-19.
30. Yu L, Takeda K, Markoff L. 2013. Protein-protein interactions among West Nile non-structural proteins and transmembrane complex formation in mammalian cells. Virology 446:365–377. https://doi.org/10.1016/j.virol.2013.08.006.
31. Bílý T, Palus M, Eyer L, Elsterová J, Vancová M, Růžek D. 2015. Electron tomography analysis of tick-borne encephalitis virus infection in human neurons. Sci Rep 5:10745. https://doi.org/10.1038/srep10745.
32. Yu C, Achazi K, Moller L, Schulzke JD, Niedrig M, Bucker R. 2014. Tick-borne encephalitis virus replication, intracellular trafficking, and pathogenicity in human intestinal Caco-2 cell monolayers. PLoS One 9:e96957. https://doi.org/10.1371/journal.pone.0096957.
33. Senigl F, Grubhoffer L, Kopecky J. 2006. Differences in maturation of tick-borne encephalitis virus in mammalian and tick cell line. Intervirology 49:239–248. https://doi.org/10.1159/000091471.
34. Růžek D, Vancová M, Tesařová M, Ahantarig A, Kopecký J, Grubhoffer L. 2009. Morphological changes in human neural cells following tick-borne encephalitis virus infection. J Gen Virol 90:1649–1658. https://doi.org/10.1099/vir.0.010058-0.
35. Pizzato M, Erlwein O, Bonsall D, Kaye S, Muir D, McClure MO. 2009. A one-step SYBR Green I-based product-enhanced reverse transcriptase assay for the quantitation of retroviruses in cell culture supernatants. J Virol Methods 156:1–7. https://doi.org/10.1016/j.jviromet.2008.10.012.
36. Wu TD, Nacu S. 2010. Fast and SNP-tolerant detection of complex variants and splicing in short reads. Bioinformatics 26:873–881. https://doi.org/10.1093/bioinformatics/btq057.
37. Anders S, Pyl PT, Huber W. 2015. HTSeq—a Python framework to work with high-throughput sequencing data. Bioinformatics 31:166–169. https://doi.org/10.1093/bioinformatics/btu638.
38. Robinson MD, McCarthy DJ, Smyth GK. 2010. edgeR: a Bioconductor package for differential expression analysis of digital gene expression data. Bioinformatics 26:139–140. https://doi.org/10.1093/bioinformatics/btp616.
39. Li J, Shi Y, Toga AW. 2015. Controlling false discovery rate in signal space for transformation-invariant thresholding of statistical maps. Inf Process Med Imaging 24:125–136. https://doi.org/10.1007/978-3-319-19992-4_10.
40. Eden E, Navon R, Steinfeld I, Lipson D, Yakhini Z. 2009. GOrilla: a tool for discovery and visualization of enriched GO terms in ranked gene lists. BMC Bioinformatics 10:48. https://doi.org/10.1186/1471-2105-10-48.